Correlation of the Magnetomechancial Coupling and Damping in $Fe_{80}Si_9B_{11}$ Metallic Glass Ribbons

Xu Zhang *, Yu Sun, Bin Yan, Xin Zhuang *

Posted Date: 30 May 2023

doi: 10.20944/preprints202305.2063.v1

Keywords: Fe-based amorphous alloys; magnetomechancial coupling; damping factor

Article

Correlation of the Magnetomechancial Coupling and Damping in $Fe_{80}Si_9B_{11}$ Metallic Glass Ribbons

X. Zhang [1,2,3,*], Y. Sun [1,2,4], B. Yan [1,2] and X. Zhuang [1,2,4,*]

[1] Aerospace Information Research Institute, Chinese Academy of Sciences, Beijing 100190, China
[2] Key Laboratory of Electromagnetic Radiation and Sensing Technology, Chinese Academy of Sciences, Beijing 100190, China
[3] School of Physical Science and Technology, Inner Mongolia University, Hohhot 010021, China
[4] University of Chinese Academy of Sciences, Beijing 100049, China
* Correspondence: zhuangxin@aircas.ac.cn, zhangxu2019@imu.edu.cn

Abstract: Understanding of the correlation between the magnetomechancial coupling factors (k) and damping factors (Q^{-1}) is a key pathway to enhance the magnetomechanical power conversion efficiency in laminated magnetoelectric (ME) composites by engineeringly manipulating the magnetic and mechanical properties of Fe-based amorphous metals. The k and Q^{-1} factors of FeSiB amorphous ribbons annealed in air at different temperatures are investigated. It is found that k and Q^{-1} factors are affected by both magnetic and elastic properties. The magnetic and elastic properties are equalized in terms of the magnetomechanical power efficiency for the low temperature annealing. The k and Q^{-1} of FeSiB-based epoxied laminates with different stacking numbers show that the -3 dB bandwidth and Young's modulus are equalized in terms of the magnetomechanical power efficiency for the high lamination stacking.

Keywords: Fe-based amorphous alloys; magnetomechancial coupling; damping factor

1. Introduction

The contradiction between human needs and technology development is still outstanding in the society of 21st century. This is due to the change of the life values with the evolution of our emotional resonance after the Cold War—we pursue a world of diversity and harmony instead of a homogeneous living environment. A high-quality development is not only the abundance in materials, but the related cost is also tremendously considered, which includes the harmfulness to the environment and human morality. The UN's sustainable development goals (SDGs) initiates the "responsible consumption and production" (SDG12) with a low carbon lifestyle [1,2]. It is implied that the R&D in highly efficient materials, devices and system is an emergency issue for nowadays [1,2].

The functionality of devices and systems are usually based on the exploration of the energy conversion in the materials that constitute those devices and systems. Thus, the energy in the transaction materials converts from one form to another to transmit the information and/or transport the power. To develop a material with high energy conversion efficiency requires balancing two or multiple parameters in it, as the relevant parameters in a material usually have impacts on each other in an extent degree [3]. To keep a parameter unchanged and balance the other parameters is normally unreasonable, it is even more struggling to balance two main parameters in some energy-converting materials. Specifically, the magnetomechanical power conversion efficiency (η) in magnetostrictive materials is based on two mutually exclusive but relative parameters—the magnetomechanical coupling coefficient (k) and damping factor (Q^{-1}) [4,5]. The two factors are concomitant in most of the magnetomechancial transduction materials. For example, the traditional annealing procedure usually causes the relative change in k and Q^{-1} factors, this implies a dwarfed η value [3,5]. To enhance the efficiency a step forward, it is needed to further clarify the correlation in the variations between k and Q^{-1} and to disrupt the fatal causality between the two factors.

 doi:10.20944/preprints202305.2063.v1

The k factor quantifies the ratio between the magnetic-to-mechanical energy conversion and the energy storage ability over a period in magnetostrictive devices [6,7]. The Q factor, a reciprocal of the damping factor, is another important parameter that quantifies the ratio between the power storage and the power loss [7,8]. The two factors can be used to characterize the magnetomechanical properties in Fe-based amorphous alloys that are ferromagnetic metallic glasses with good magnetic and magnetomechanical properties[4]. One of the recent applications of high efficiency Fe-based amorphous alloys have been whispered to the magnetoelectric (ME) laminated composites that contains the ferromagnetic glassy metals and the piezoelectric layers[3]. The ME composites have been recognized as one of the most promising candidates for practical applications in many devices due to their much higher ME coupling than single-phase materials [9–11]. The relevant applications include the magnetic field sensors, the radio signal processing devices, the novel magnetic memory elements and the autonomous power sources [12–15].

The magnetic and mechanical properties of the amorphous alloys are essential parameters to achieve high performance for their utilizing in ME composites. To optimize the magnetomechanical properties of metallic glassy ribbons in such devices, the heat treatment has been investigated to adjust both magnetic properties and mechanical properties [4,16–18]. The influence of annealing on the magnetic properties of Fe-based amorphous ribbon have been vastly studied. The annealing procedure can adjust the saturation magnetic flux density (B_s), coercivity (H_c), permeability (μ_r), k, Q and η factors, but the variation of these parameters is rarely independent [3,4,8,19–38]. Thus, a huge room has been reserved for the researchers to cooperatively elevate two or multiple parameters while causing the least negative impact. In this study, the influence of heat treatment on the magnetomechancial properties for FeSiB amorphous ribbons is investigated. The correlation of k and Q (or Q^{-1}) factors of such ribbons that were annealed at temperatures far below the crystallization temperature is discussed. The magnetic properties and magnetomechancial properties in the single-foil ribbons and epoxy-ribbon laminates are also measured and compared in this work.

2. Experiment method

The samples used in this work to perform the experiments are Fe-based amorphous ribbons with a nominal composition of $Fe_{80}Si_9B_{11}$ (at%). The width of the ribbons is 5 mm while the thickness is approximately 25 μm. The ribbons were cut into rectangular shape with a length of 40 mm and then annealed at different temperatures in air for 20 minutes using a muffle furnace. The annealed ribbons were inserted into a rectangular solenoid coil with a dimension of around 40×10×10 mm^3. Since the impedance and inductance values were extremely sensitive to the applied dc field to amorphous ribbons [39,40] when they were driven by a magnetic excitation near the mechanical resonant frequency [41,42]. The inductance of the coils with inserted ribbon were measured by a high-precision impedance analyzer (HP 4294A). The resonant frequencies (f_r at maximum impedance) and anti-resonant frequencies (f_a at minimum impedance) on the motion impedance curve were also measured by the impedance analyzer under a dc magnetic bias field (H_{dc}) along the longitudinal direction of the ribbons [43,44]. The values of k are determined using resonant and anti-resonant frequencies, Q can be directly measured by the two poles (f_1 at maximum inductance, f_2 at minimum inductance) vs frequency [4,8,44]. From the frequency at f_r, f_a, f_1 and f_2 the values of k and Q are calculated using the following dependences: $k = \sqrt{(\pi^2/8)(1 - f_r^2/f_a^2)}$ and $Q = f_r/(f_2 - f_1)$, where $\Delta f = f_2 - f_1$ is also corresponding to the -3 dB bandwidth near the resonance [8]. The schematic diagram of the experiment is shown in Fig. 1.

Preprints (www.preprints.org) | NOT PEER-REVIEWED | Posted: 30 May 2023 doi:10.20944/preprints202305.2063.v1

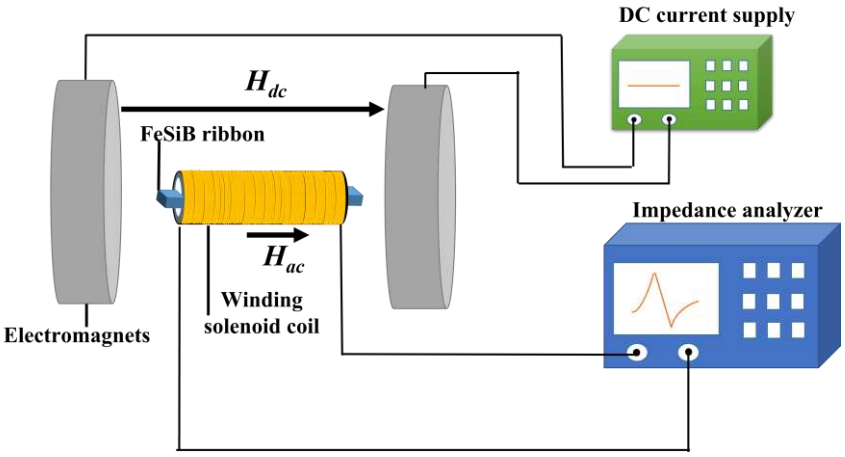

Figure 1. Schematic diagram of the experiment.

The measured inductance (L) values of the winding coil with an inserted Fe-based ribbon are linearly proportional to the magnetic permeability of the ribbon core due to the high magnetic susceptivity of the ribbon, following the expression: $L = N^2 \mu_0 \mu_r S / l$ [45], where μ_0 and μ_r are the magnetic permeability of vacuum and the ribbon, respectively. N is the number of rounds of the wire for the coil. S is the cross section aera of the coil. l is the length of the coil. The values of Young's modulus (E) in the ribbons with a length match to the coil can be calculated from the measured values of the anti-resonant frequency: $f_a = (2l)^{-1}(E/\rho)^{0.5}$,where l is the length of the ribbon, ρ is the density of the ribbon, respectively [8,37,46]. The magnetic hysteresis loops of the ribbons annealed at different temperatures are measured by using the vibrational sample measurement system (VSM, MicroSense EZ-7). The samples with a dimension of around 5×5×0.025 mm^3 are prepared together in the furnace with the 40mm long ribbons for VSM measurements.

3. Theoretical analysis and Measurement

a) Eddy current loss

The equivalent input loss factor (ξ) has been defined as the inverse of the product of k^2 and Q. It quantifies the ratio between the power conversion and the power loss in the magnetic-to-mechanical energy conversion. Following the previous investigations [4,8,35,37,47], ξ can be written as

$$\xi = \frac{1}{k^2 Q} = c_e \mu_0 \chi f_r + \frac{1}{k^2 Q_0} \tag{1}$$

where c_e is the loss coefficient for the eddy current, χ is the magnetic susceptibility of the ribbons, Q_0 is the quality factor under magnetostriction-free conditions. From the right-hand side of Eq. (1), the first term with c_e represents the energy loss for dynamic magnetization procedure, which is affected by the magnetic properties of the ribbon, the second part represents the loss not related to the eddy current. In single ribbons, the eddy current loss dominates after the heat treatment under the annealing temperature far below the crystallization temperature. Following Herzer *et al.* [48], the formula of c_e is expressed as

$$c_e = \frac{(\pi t)^2}{6\rho_{el}} \left(1 + \frac{w^2}{(w\cos\beta + t)^2} \frac{m^2}{1-m^2} \right) \tag{2}$$

Preprints (www.preprints.org) | NOT PEER-REVIEWED | Posted: 30 May 2023 doi:10.20944/preprints202305.2063.v1

where t is the ribbon thickness, ρ_{el} is the electric resistivity, β is the angle between the average magnetic anisotropy and the ribbon direction. $m = J_H / J_s$ is the averaged longitudinal magnetization (J_H) normalized to the saturation magnetization (J_S). w is the magnetic domain width, the formula is given as [48]

$$w^2 = \frac{8L_{ex}t}{N_{zz}\sin^2\beta + N_{yy}\cos^2\beta} \tag{3}$$

where $L_{ex} = \sqrt{A/K}$ is the magnetic exchange length. A is defined as the exchange stiffness and K is the anisotropy constant. N_{zz} and N_{yy} are demagnetization factors along the longitudinal and width direction of the ribbon, respectively. With the help of Eq. (2) and (3), the contribution of the eddy current in Eq. (1) can be rewritten as

$$\xi_{eddy} = \frac{(\pi t)^2}{6\rho_{el}}\mu_0\chi f_r + \frac{(\pi t)^2}{6\rho_{el}}\frac{m^2}{1-m^2}\frac{w^2}{(w\cos\beta + t)^2}\mu_0\chi f_r \tag{4}$$

Taking into account that the average anisotropy angle β is close to zero for the ribbons annealed at low temperatures, Eq. (4) is rewritten as

$$\xi_{eddy} = \frac{(\pi t)^2}{6\rho_{el}}\mu_0\chi f_r + \frac{\pi^2}{6\rho_{el}}\frac{m^2}{1-m^2}\left(\frac{1}{t}+\frac{1}{w}\right)^{-2}\mu_0\chi f_r \tag{5}$$

When the magnetic domain width is usually much larger than the ribbon thickness in low-temperature annealed samples, the assumption $w >> t$ can be considered in the calculation. Thus, Eq. (5) can be rewritten as

$$\xi_{eddy} = \frac{1}{k^2 Q} = \frac{(\pi t)^2}{6\rho_{el}}\left(1 + \frac{m^2}{1-m^2}\right)\mu_0\chi f_r \tag{6}$$

The equivalent loss factor induced by the eddy current loss for the ribbons annealed at low temperature depends only on the variation of χ and f_r for the ribbons.

b) Magnetic and magnetomechancial properties

The hysteresis loops of magnetic materials could provide important information on the magnetic properties of materials. Fig. 2(a) shows the dc magnetic hysteresis loops of the samples annealed in air at different annealing temperatures (T_{AN}) for 20 minutes. The loops show small values of remnant magnetization and H_c for all the samples, suggesting that the samples remain good soft magnetic properties after the heat treatment in air. As shown in the inset in Fig. 2(a), the values of H_c basically stay close to 0.1 Oe in the region of T_{AN} from 370 °C to 450 °C. However, H_c begins to grow sharply with the increase of T_{AN} when T_{AN} exceeds 450 °C. In this case, the change of the chemical concentration causing the ordered clusters, the subsequent topological and chemical long-range orderings on the surface of the ribbons results in the variations in the values of H_c [31,33,34,36,47,49]. When T_{AN} is above 500 °C, H_c shows a burst increase which suggests further deterioration in the soft magnetic properties. This is due to (1) the increasing fraction of the surface crystallization at high T_{AN}; (2) a film of boron oxides formed with excessive boron atoms which are separated from the α-Fe crystallites, since the α-Fe crystallites have much lower solubility of B than that of amorphous Fe [4,22,28,31,33,36]. Consequently, the magnetic domains in the amorphous remainders are thinned and turned to the out-of-plan direction by the compress stress that are induced by the surface crystallization and surface oxidation films [4,22,28,31,33,36], leading to the increasing of H_c.

Preprints (www.preprints.org) | NOT PEER-REVIEWED | Posted: 30 May 2023 doi:10.20944/preprints202305.2063.v1

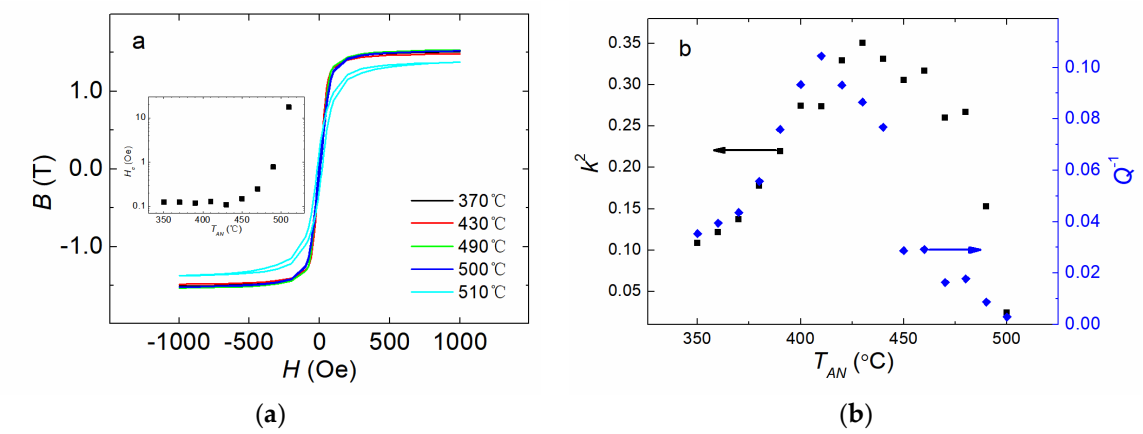

(a) (b)

Figure 2. (a) The hysteresis loops of FeSiB amorphous ribbons obtained after annealed at different temperatures from 370 °C to 510 °C for 20 minutes in air, the inset figure is the annealing temperature (T_{AN}) dependence of coercivity H_c. (b) Damping factors (Q^{-1}) and the square of magnetomechanical coupling (k) as a function of T_{AN} for 20 minutes in air. k is acquired at its maximal values with external dc magnetic bias field H_{dc}. The values of Q^{-1} are measured under the same H_{dc} when k is maximized.

In our previous work, we have reported the T_{AN} dependency of k and Q for single FeSiB ribbons, the value of k reaches its maximum around T_{AN} of 430 °C, while Q shows a minimal value around T_{AN} of 410 °C [4]. The k^2 and Q^{-1} evolution after annealed at various temperature T_{AN} are shown in Fig. 2(b). In low T_{AN} region below 400 °C, with increasing T_{AN}, k^2 increases while Q^{-1} decreases at almost the same pace, indicating k^2 and Q^{-1} are correlated in low annealing temperature region. For higher T_{AN} from 400 °C to 500 °C, the variation of k^2 and Q^{-1} become non-synchronous, indicating the correlation level of these parameters drops significantly. As a result of synchronous change of k^2 and Q^{-1} for low T_{AN} below 400 °C, the equivalent input loss ξ stays almost invariable for low T_{AN} below 400 °C, as reported by our earlier investigations [4].

c) Softening of magnetic and elastic properties

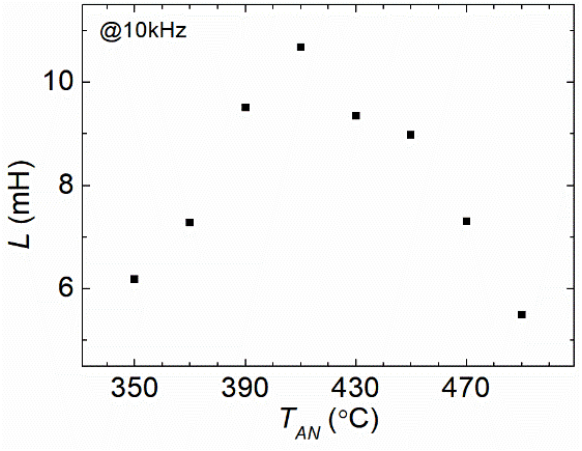

Figure 3. The variation of inductance (L) of the winding coil with an inserted FeSiB ribbon annealed for 20 minutes at different annealing temperatures T_{AN} from 350 °C to 490 °C. The measured L is linearly proportional to the magnetic permeability of the ribbon core due to the high magnetic susceptivity of the ribbon, following the expression: $L = N^2 \mu_0 \mu_r S / l$, where μ_0 and μ_r are the magnetic permeability of vacuum and the ribbon, respectively. N is the number of rounds of the wire for the coil. S is the cross section aera of the coil. l is the length of the coil.

Fig. 3 shows the measured values of the inductance (L) at 10 kHz after isothermal annealing at various temperature T_{AN}, it can be observed that L increases with T_{AN} in the region from 350 °C to 410

Preprints (www.preprints.org) | NOT PEER-REVIEWED | Posted: 30 May 2023 doi:10.20944/preprints202305.2063.v1

°C, then decreases for T_{AN} from 420 °C to 490 °C. According to the formula $L = N^2 \mu_0 \mu_r S / l$, the values of L are proportional to the magnetic permeability (μ_r) of the ribbon. Similar behavior of μ_r can also be observed from the magnetic hysteresis loops in Fig. 1(a).

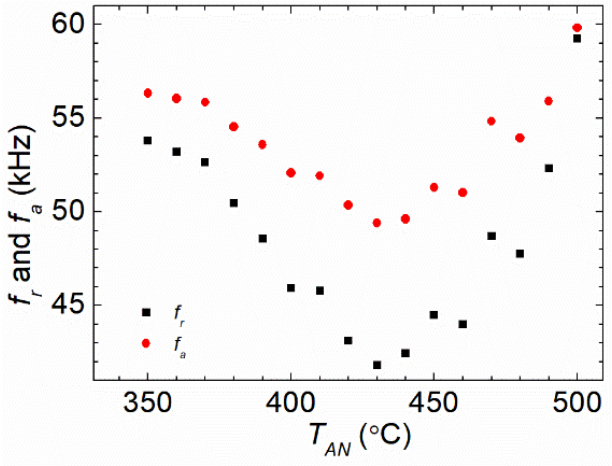

Figure 4. The variation of the resonant frequencies (f_r) and anti-resonant frequencies (f_a) of the winding coil with an inserted FeSiB ribbon annealed for 20 minutes at different annealing temperatures T_{AN} from 350 °C to 500 °C. The f_r and f_a on the motion impedance curve were measured by the impedance analyzer under an dc magnetic bias field (H_{dc}) along the longitudinal direction of the ribbons. The values of Young's modulus (E) in the ribbons with a length match to the coil can be calculated from the measured values of the anti-resonant frequency: $f_a = (2l)^{-1}(E/\rho)^{0.5}$,where l is the length of the ribbon, ρ is the density of the ribbon, respectively [8,37,46].

Fig. 4 shows the T_{AN} dependence of resonant f_r and anti-resonant f_a. It can be observed that in low T_{AN} region, both f_r and f_a decrease with the increase of T_{AN} and reach a minimal value at 410 °C. Then they rise as T_{AN} continues to increase. Following the formula of $f_a = (2l)^{-1}(E/\rho)^{0.5}$, the values of f_a is related to E of the ribbon [8]. Besides, it can be observed in Fig. 4 that f_r-curve and f_a-curve has almost the same pattern and the similar amplitudes, which indicates that f_r also reflects the change of E. By comparing the behavior of L and f_a (f_r) versus T_{AN}, it can be noticed that the two parameters exhibit a respective extreme value as the function of T_{AN}. However, the curves of L and f_a show a lag of 20 °C versus T_{AN} to reach their max/min values.

By comparing the T_{AN}-dependence of L with T_{AN}-dependence of Q^{-1} factors, it can be observed that the variations of L and Q^{-1} with the increase of T_{AN} are almost the same below 400 °C, the f_a (f_r) has similar profile with k factor. According to Eq. (6), the trend of k and Q are recognized as the competition of the magnetic and mechanical properties, χ and f_a (f_r). Since the L-curve and Q^{-1}-curve shares the same trend and same extreme value point of T_{AN} below 410 °C, while f_a (f_r)-curve and k-curve show the inverse trend and same extreme value point of T_{AN} below 430 °C, it is probable that L or μ_r is dominant on the values of Q^{-1} factors while f_a (f_r) or E has the dominative effect on k factor for the low T_{AN} below 410 °C (for L and Q) or 430 °C (for f_a and k).-Moreover, because k and E are related to each other, the annealing experience though α-relaxation has an important influence on the softening in elasticity below 430 °C [4]. For higher T_{AN}, because of the emerging of the surface crystallization and the long-range chemical orderings with B oxidation during the annealing procedure, the competition of magnetism and elasticity becomes much more complex, leading to the divorce between k^2-curve and Q-curves as well as between f_a (f_r)-curve and L-curve versus T_{AN} [4,31,33,34,36,38,47].

Below 410 C-T_{AN}, the β-relaxation in Fe-lack zones was dominant and lead to the chemical short-range ordering (CSRO) in Fe-rich zones with the doped B atoms by diffusion[4]. In addition, the topological short-range ordering (TSRO) also occurs at this low T_{AN} region as another result of β-relaxation, leading to the releasing of internal stress, both of which alleviate the pinning effect of the magnetic domain by defects in the sample [4], the expanding speed of magnetic domain increase

Preprints (www.preprints.org) | NOT PEER-REVIEWED | Posted: 30 May 2023 doi:10.20944/preprints202305.2063.v1

therefor, i.e. L (μ_r) increases. For T_{AN} from 450 °C to 500 °C, the sharp decrease of L (μ_r) may be due to the emerging of surface crystallization together with more severe surface oxidation that leads to the apparency of the grain boundary as well as magnetic anisotropy deviating from the long axis direction, both of which inhibit the movement or rotation of the magnetic moment of the magnetic domain, resulting in the smaller variation rate of the magnetic moment. The increase of H_c above 450 °C also coincides with the decrease of L (μ_r), suggesting the deterioration of the soft magnetic properties in high T_{AN} region.

The decrease of E in the low T_{AN} region suggests that the deformation quantity of the ribbon becomes smaller with the increasing T_{AN}. According to previous studies [4,38], as a result of β-relaxation for low T_{AN}, besides of the increasing of Fe-Fe bond caused by the CSRO, the TSRO could also be triggered by β-relaxation close to the cluster-matrix boundaries. The TSRO brings a decrease in the ductility of the sample, thus the sample becomes "more flexible" to be stretched. Consequently, E (f_a and f_r) becomes smaller after annealed at relatively low temperature and reaches minimum at 430 °C, as shown in Fig. 4. The E (f_a and f_r) vs. T_{AN} curve switches to an increasing trend when T_{AN} exceeds 430 °C. This can be attributed to the apparency of α-relaxation, which is more intensive and usually occurs at high T_{AN}. This α-relaxation further enhances the diffusion of the atoms, affecting the atomic orderings in a larger scale and usually reshaping the clusters. Fe or metalloid atoms experiencing a long-term relaxation in the B-rich area leads to the generation of some clusters with high elasticity that increase the values of E. In addition, because the annealing procedure in this article is taken in air, the oxidation is more strongly and penetrates deeper in the ribbons at high T_{AN}, this also has a strong influence on the rigidity of the ribbon [4,20].

From Fig. 3 and Fig. 4, it can be obtained that the variation trends of magnetic susceptibility χ (χ is also proportional to L in Fig. 3) and resonant (anti-resonant) frequency f_r (f_a) are synchronous but opposite for low T_{AN} from 350 °C to 400 °C, the product of χ and f_r (f_a) remains close to a constant. Besides, the measured η, relating to k^2Q, is nearly a constant value in this region of T_{AN} following our previous investigations[4,25]. Therefore, according to Eq. (1), it could be inferenced that the loss factor c_e which represents the eddy current loss should be basically unchanged for low T_{AN} from 350 °C to 400 °C for the single FeSiB ribbons. This is consistent with our analysis in the theoretical section as well.

When T_{AN} approaches to the crystallization temperature (T_x) of the FeSiB glassy metals, the size of the magnetic domain decreases due to the change of surface stress [4,34,36]. According to Herzer *et al.* [4,8,35,37,47,49], the loss factor c_e is related to the width of magnetic domain w, following the Eq. (2). Therefore, the synchronously changing behavior of k^2 and Q^{-1} suggest that the improvement of the soft magnetic properties may derive from the increase of the numbers of the activated magnetic units rather than the variation of the width of magnetic domains in low T_{AN} region. Thus, the values of ξ for the ribbons annealed at low T_{AN} remaining constant is more due to the increase of the quantity of magnetic units, rather than the change in the domain size.

d) Time-Temperature equivalence for the annealing

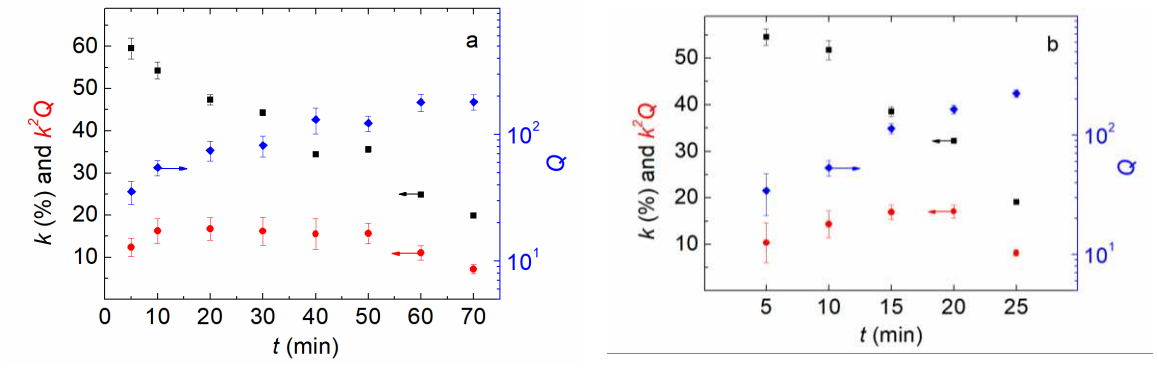

Figure 5. The magnetomechanical coupling coefficient (k) for FeSiB ribbons as a function of the annealing time (t_{AN}) at annealing temperature of (a) 470 °C and (b) 490 °C. The blue and red curves

Preprints (www.preprints.org) | NOT PEER-REVIEWED | Posted: 30 May 2023 doi:10.20944/preprints202305.2063.v1

represent the values of the quality factors (Q) and efficiency factors (k^2Q) associated to the maximum values of coupling coefficient k, respectively.

Fig. 5 (a) and (b) displays the variation of k, k^2Q and Q factor for different annealing times t_{AN} at T_{AN} from 470 °C to 490 °C, respectively. A significant decrease of k factor with the increase of Q factor occurs with the increase of t_{AN} for T_{AN} of 470 °C and 490 °C. The curve of k and Q show a cross profile at t_{AN} = 40 minute and 15 minutes, respectively. After the ribbons are annealed for 40 minutes at T_{AN} = 470 °C and 15 minutes at T_{AN} = 490 °C, k decreases approximately from 60% to 40%, while the values of Q increase close to 200. The equivalent input loss factors ξ show a max value when t_{AN} is 20 minutes for both samples, which suggests the optimal annealing time for the annealing at 470 °C and 490 °C. Based on the data mentioned above, it is implied that the decrease in k is caused by the surface oxidation and surface crystallization that induces the increase of the coercivity by the out-of-plane magnetic anisotropy. The increase of Q factors might be due to the long range-orderings that take place in the surface regions of the ribbons.

The Q factor represents the quality of mechanical performance in our FeSiB ribbons, a high value in Q factor indicates a high ratio between the storage power to the power loss. From Fig. 5(a) and (b), it can be observed that the overall trend of k, k^2Q and Q curves at 470 °C T_{AN} are similar to that at 490 °C T_{AN}, separately. Besides, the increase of T_{AN} from 470 °C to 490 °C narrows the T_{AN} window before the magnetomechanical properties deteriorate obviously. In terms of the η factors, it is similar to increase T_{AN} for a constant t_{AN} or to increase t_{AN} at a fixed T_{AN}, which suggests that T_{AN} and t_{AN} have equal effect on the η factor in the heat treatment procedure for the FeSiB ribbons to some extent. However, the equivalence of t_{AN} and T_{AN} in terms of the magnetomechanical power conversion efficiency seems to exist only at relative higher T_{AN}, we do not observe this equivalence with T_{AN} below 400 °C.

e) Magnetomechancial properties in epoxy-ribbon composites

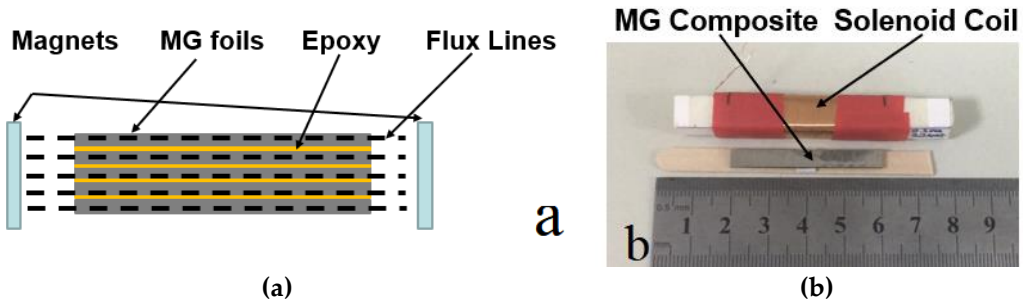

Figure 6. (a) Schematic diagram of a laminated composite consisting of magnetostrictive amorphous FeSiB ribbons bonded by epoxy resin. (b) Photo of laminated metallic glass (FeSiB) ribbon composites and the solenoid coil used to generate the ac magnetic field.

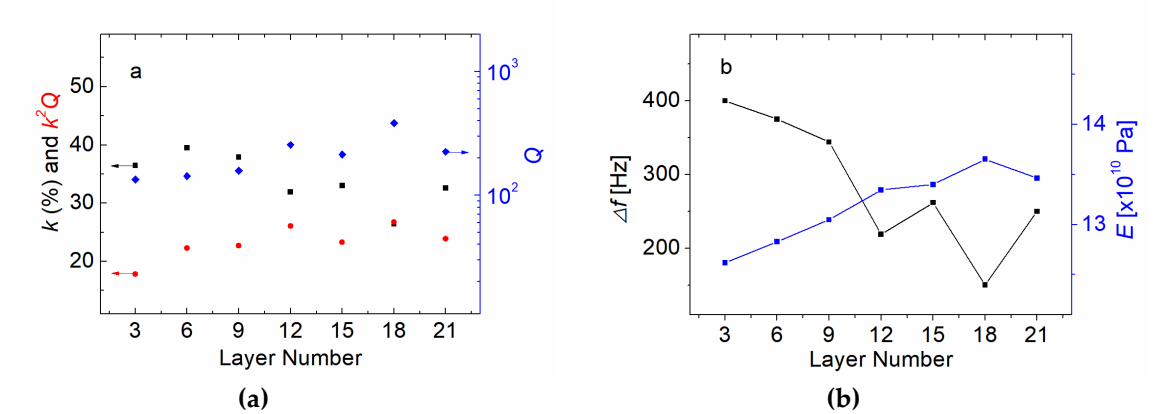

Figure 7. (a) The black curve is the magnetomechanical coupling factor (k) for laminated metallic glass composites consisting of magnetostrictive amorphous FeSiB ribbons as a function of the FeSiB-layer

 doi:10.20944/preprints202305.2063.v1

numbers. The blue and red curves represent the values of the quality factors (Q) and efficiency coefficients (k^2Q) associated to the maximum values of coupling coefficient k, respectively. (b) The trend of the -3 dB bandwidth (Δf) and Young's modulus (E) for laminated FeSiB ribbon composites as a function of the FeSiB-layer number, where $\Delta f = f_2 - f_1$ (f_1 at maximum inductance, f_2 at minimum inductance).

A schematic diagram of a laminated composite consisting of magnetostrictive amorphous FeSiB ribbons bonded by epoxy resin is given in Fig. 6(a). Several FeSiB foils are fabricated by using hot-pressing techniques and an A-B part epoxy. The should-be ratio between the epoxy (A part) and the curing agent (B part) is 3:1. Fig. 6(b) is a photo of the laminated FeSiB composites, we apply a dc magnetic field along the laminated composite, as shown in the upper part of Fig. 6(b). The ratio between the quantity of magnetostrictive layers and the quantity of epoxy resin is varied to investigate the change of k, Q, and k^2Q in FeSiB laminated composites with different foil numbers. The results are given in Fig. 7(a). It is found that as the number of FeSiB layers increases, the k factors increase slightly and then decrease rapidly, while the Q factors show an overall increase trend to a maximum close to 400, corresponding to a foil number from 18 to 21 in the FeSiB laminates. The efficiency factor k^2Q firstly increases for more FeSiB ribbons layers, and then reaches a relatively stable value around 25 corresponding to the FeSiB foil number from 12 to 21. Fig. 7(b) shows the trend of the -3 dB bandwidth (Δf) and E for the FeSiB laminated composites with different foil numbers.

In Fig. 7(a), it is observed that when the foil number is small, there is no obvious similarity or correlation between the k and Q factors as FeSiB layer numbers varies. The k and Q in the laminated composites with 9-layers, 6-layers, and 3-layers of FeSiB ribbons are examples. But for the laminated composites with more foil number of 12-layers, 15-layers, 18-layers and 21-layers, the data suggest that there is a mutually exclusive relationship between the k and Q factors. This causes the k^2Q factors reaching a relatively stable state and that the k^2Q factors does not continue increasing with the increase of the FeSiB layer number. For the record, it is needed to particularly emphasize that the ratio between epoxy and curing agents is *not* 3:1. The amount of the curing agent is reduced, giving a ratio less than 3:1 between the epoxy and the curing agent, so the epoxy resin was not fully solidified for the laminated samples. Thus, the mechanical loss due to the inter-friction is increased comparing to the samples with fully cured epoxy. Unlike the eddy current loss in the single-foil ribbons, the dominant loss in the FeSiB laminates is ascribed to the mechanical loss that triggers the temperature rising when the laminated composites are driven under high power conditions.

According to previous research, as T_{AN} approaches to T_x, the size of the magnetic domain decreases due to the change of surface stress [4,34]. As mentioned above, the efficiency of a single-foil ribbon experienced a low T_{AN} remains constant, and this is more due to the increasing of the number of the magnetic units, rather than the change in the magnetic domain size. In contrast, the increase of the k^2Q factors at T_{AN} above 450 °C is due to the reduction of magnetic domains size. Following the Eq. (1), because the k^2Q factors of the laminated FeSiB composites is approximately a constant for high layer number laminates, and because the variation trend of E (associated to f_r and f_a) and the bandwidth (associated with χ) of the laminated FeSiB composites remains consistent with each other for all the foil numbers, c_e of the laminated composites should remain constant, too. As the foil number of the FeSiB laminates decreases, the volume proportion of magnetostrictive materials (FeSiB) in laminated composite gradually increases. Using similar analyzing principle to Fig. 7(a), the reason for the constant values in k^2Q factors for the ribbons with the foil number from 12 to 21 is probably due to the increase in the number of ribbons, rather than the change in the relative fraction of the ribbons. The reason for the change in the k^2Q factors for the laminates with the foil number from 3 to 12 is due to the variation of the relative volume fraction of FeSiB ribbons, but rather than the variation in the ribbon number. That is to say, the change in k^2Q factors between the laminates with the ribbon number from 3 to 12 derives from the relative size of the magnetic units, which corresponds to the relative volume fraction of FeSiB ribbons in the laminates; while the constant k^2Q factors between the 12-layers and 21-layers laminates come from the change in the number of magnetic units, rather than the change in relative volume of magnetic units.

5. Conclusions

In summary, we investigated the influence of magnetic and elastic properties on magnetomechancial coupling factors (k) and damping factors (Q^{-1}) by measuring the resonant and anti-resonant frequencies from the motion impedance and the inductance spectrum from a winding coil with an annealed-FeSiB ribbon. We can draw the following conclusions:

1. By experiencing the annealing under different temperatures, the dynamic magnetic and elastic properties in the $Fe_{80}Si_9B_{11}$ ribbons vary correlatively with the annealing temperature. However, the resonant frequency reaches its minimum value at 430 °C with a lag of 20 °C when the magnetic parameter reaches its minimum at 410 °C, coinciding with the behaviors of k and Q^{-1} when the annealing temperature changes.

2. It is found that annealing temperature and annealing time has equally impact in the heat treatment procedure for the FeSiB ribbons to maximize the magnetomechancial power efficiency. But the equivalence is correct only when the annealing temperature is high enough that the long-range orderings can occur in the surface region of the ribbons.

3. The investigation of the FeSiB laminated composites suggests that the behavior of k and Q^{-1} factors in the laminates with the various foil number from 12 to 21 is like the behaviors of k and Q^{-1} factors in the single-foil FeSiB ribbons with various annealing temperature from 350 °C to 400 °C.

Author Contributions: Conceptualization, X.Z. (Xin Zhuang); methodology, X.Z. (Xin Zhuang), X.Z. (Xu Zhang); software, X.Z. (Xin Zhuang), X.Z. (Xu Zhang); validation, X.Z. (Xin Zhuang), X.Z. (Xu Zhang),; formal analysis, X.Z. (Xin Zhuang), X.Z. (Xu Zhang); investigation, X.Z. (Xin Zhuang), X.Z. (Xu Zhang); resources, X.Z. (Xin Zhuang), X.Z. (Xu Zhang); data curation, X.Z. (Xin Zhuang), X.Z. (Xu Zhang); writing—original draft preparation, X.Z. (Xu Zhang); writing—review and editing, X.Z. (Xin Zhuang), X.Z. (Xu Zhang), Y.S. and B.Y.; visualization, X.Z. (Xin Zhuang), X.Z. (Xu Zhang); supervision, X.Z. (Xin Zhuang); project administration, X.Z. (Xin Zhuang), X.Z. (Xu Zhang); funding acquisition, X.Z. (Xin Zhuang), X.Z. (Xu Zhang) All authors have read and agreed to the published version of the manuscript."

Funding: This research was funded by the National Key R & D Program of China: No. 2021YFA0716500, the Natural Science Foundation of Inner Mongolia: No. 2021BS05010 and the talent program with Chinese Academy of Sciences.

Institutional Review Board Statement: Not applicable.

Informed Consent Statement: Not applicable.

Data Availability Statement: Not applicable.

Conflicts of Interest: The authors declare no conflict of interest.

References

1. Papadopoulou, C.-A. Chapter 4 - Technology and SDGs in Smart Cities Context. In *Smart Cities and the un SDGs*; Visvizi, A., Pérez del Hoyo, R., Eds.; Elsevier, 2021; pp. 45–58 ISBN 978-0-323-85151-0.
2. Ortiz-Repiso, V. Chapter 11 - The 2030 Agenda and the Information Professionals. In *Boosting the Knowledge Economy*; Calzada-Prado, F.-J., Ed.; Chandos Information Professional Series; Chandos Publishing: Oxford, 2022; pp. 189–208 ISBN 978-1-84334-772-9.
3. Channagoudra, G.; Dayal, V. Magnetoelectric Coupling in Ferromagnetic/Ferroelectric Heterostructures: A Survey and Perspective. *J Alloys Compd* **2022**, *928*, doi:10.1016/j.jallcom.2022.167181.
4. Zhuang, X.; Xu, X.; Zhang, X.; Sun, Y.; Yan, B.; Liu, L.; Lu, Y.; Zhu, W.; Fang, G. Tailoring the Magnetomechanical Power Efficiency of Metallic Glasses for Magneto-Electric Devices. *J Appl Phys* **2022**, *132*, doi:10.1063/5.0098282.
5. Leung, C.M.; Li, J.; Viehland, D.; Zhuang, X. A Review on Applications of Magnetoelectric Composites: From Heterostructural Uncooled Magnetic Sensors, Energy Harvesters to Highly Efficient Power Converters. *J Phys D Appl Phys* **2018**, *51*, 263002, doi:10.1088/1361-6463/aac60b.
6. Kabacoff, L.T. Thermal, Magnetic, and Magnetomechanical Properties of Metglas 2605 S2 and S3. *J Appl Phys* **1982**, *53*, 8098–8100, doi:10.1063/1.330270.
7. Savage, H.; Clark, A.; Powers, J. Magnetomechanical Coupling and ΔE Effect in Highly Magnetostrictive Rare Earth - Fe2compounds. *IEEE Trans Magn* **1975**, *11*, 1355–1357, doi:10.1109/TMAG.1975.1058791.

8. Kaczkowski, Z. Magnetomechanical Properties of Rapidly Quenched Materials. *Materials Science and Engineering: A* **1997**, *226–228*, 614–625, doi:https://doi.org/10.1016/S0921-5093(96)10695-X.
9. Qiao, K.; Hu, F.; Zhang, H.; Yu, Z.; Liu, X.; Liang, Y.; Long, Y.; Wang, J.; Sun, J.; Zhao, T.; et al. Unipolar Electric-Field-Controlled Nonvolatile Multistate Magnetic Memory in FeRh/(001)PMN-PT Heterostructures over a Broad Temperature Span. *Sci China Phys Mech Astron* **2021**, *65*, 217511, doi:10.1007/s11433-021-1779-0.
10. Pal, M.; Srinivas, A.; Asthana, S. Enhanced Magneto-Electric Properties and Magnetodielectric Effect in Lead-Free (1-x)0.94Na0.5Bi0.5TiO3-0.06BaTiO3–x CoFe2O4 Particulate Composites. *J Alloys Compd* **2022**, *900*, 163487, doi:https://doi.org/10.1016/j.jallcom.2021.163487.
11. Li, T.X.; Li, R.; Lin, Y.; Bu, F.; Li, J.; Li, K.; Hu, Z.; Ju, L. Study of Enhanced Magnetoelectric Coupling Behavior in Asymmetrical Bilayered Multiferroic Heterostructure with Two Resonance Modes. *J Alloys Compd* **2022**, *895*, 162674, doi:https://doi.org/10.1016/j.jallcom.2021.162674.
12. Röbisch, V.; Salzer, S.; Urs, N.O.; Reermann, J.; Yarar, E.; Piorra, A.; Kirchhof, C.; Lage, E.; Höft, M.; Schmidt, G.U.; et al. Pushing the Detection Limit of Thin Film Magnetoelectric Heterostructures. *J Mater Res* **2017**, *32*, 1009–1019, doi:10.1557/jmr.2017.58.
13. Betal, S.; Saha, A.K.; Ortega, E.; Dutta, M.; Ramasubramanian, A.K.; Bhalla, A.S.; Guo, R. Core-Shell Magnetoelectric Nanorobot – A Remotely Controlled Probe for Targeted Cell Manipulation. *Sci Rep* **2018**, *8*, 1755, doi:10.1038/s41598-018-20191-w.
14. Narita, F.; Fox, M. A Review on Piezoelectric, Magnetostrictive, and Magnetoelectric Materials and Device Technologies for Energy Harvesting Applications. *Adv Eng Mater* **2018**, *20*, 1700743, doi:https://doi.org/10.1002/adem.201700743.
15. Gao, J.; Das, J.; Xing, Z.; Li, J.; Viehland, D. Comparison of Noise Floor and Sensitivity for Different Magnetoelectric Laminates. *J Appl Phys* **2010**, *108*, 084509, doi:10.1063/1.3486483.
16. Chen, H.S.; Leamy, H.J.; Barmatz, M. The Elastic and Anelastic Behavior of a Metallic Glass. *J Non Cryst Solids* **1971**, *5*, 444–448, doi:https://doi.org/10.1016/0022-3093(71)90044-5.
17. Morito, N.; Egami, T. Correlation of the Shear Modulus and Internal Friction in the Reversible Structural Relaxation of a Glassy Metal. *J Non Cryst Solids* **1984**, *61–62*, 973–978, doi:https://doi.org/10.1016/0022-3093(84)90669-0.
18. Soshiroda, T.; Koiwa, M.; Masumoto, T. The Internal Friction and Elastic Modulus of Amorphous Pd–Si and Fe–P–C Alloys. *J Non Cryst Solids* **1976**, *22*, 173–187, doi:https://doi.org/10.1016/0022-3093(76)90017-X.
19. Xu, D.D.; Zhou, B.L.; Wang, Q.Q.; Zhou, J.; Yang, W.M.; Yuan, C.C.; Xue, L.; Fan, X.D.; Ma, L.Q.; Shen, B.L. Effects of Cr Addition on Thermal Stability, Soft Magnetic Properties and Corrosion Resistance of FeSiB Amorphous Alloys. *Corros Sci* **2018**, *138*, 20–27, doi:10.1016/j.corsci.2018.04.006.
20. Lin, J.; Li, X.; Zhou, S.; Zhang, Q.; Li, Z.; Wang, M.; Shi, G.; Wang, L.; Zhang, G. Effects of Heat Treatment in Air on Soft Magnetic Properties of FeCoSiBPC Amorphous Core. *J Non Cryst Solids* **2022**, *597*, doi:10.1016/j.jnoncrysol.2022.121932.
21. Murugaiyan, P.; Mitra, A.; Jena, P.S.M.; Mahato, B.; Ghosh, M.; Roy, R.K.; Panda, A.K. Grain Refinement in Fe-Rich FeSiB(P)NbCu Nanocomposite Alloys through P Compositional Modulation. *Mater Lett* **2021**, *295*, doi:10.1016/j.matlet.2021.129852.
22. Fang, Z.; Nagato, K.; Liu, S.; Sugita, N.; Nakao, M. Investigation into Surface Integrity and Magnetic Property of FeSiB Metallic Glass in Two-Dimensional Cutting. *J Manuf Process* **2021**, *64*, 1098–1104, doi:10.1016/j.jmapro.2021.02.026.
23. Wang, C.; Guo, Z.; Wang, J.; Sun, H.; Chen, D.; Chen, W.; Liu, X. Industry-Oriented Fe-Based Amorphous Soft Magnetic Composites with SiO2-Coated Layer by One-Pot High-Efficient Synthesis Method. *J Magn Magn Mater* **2020**, *509*, doi:10.1016/j.jmmm.2020.166924.
24. Cheng, Y.Q.; Ma, E. Atomic-Level Structure and Structure-Property Relationship in Metallic Glasses. *Prog Mater Sci* **2011**, *56*, 379–473, doi:10.1016/j.pmatsci.2010.12.002.
25. Sun, Y.; Zhang, X.; Wu, S.; Zhuang, X.; Yan, B.; Zhu, W.; Dolabdjian, C.; Fang, G. Magnetomechanical Properties of Fe-Si-B and Fe-Co-Si-B Metallic Glasses by Various Annealing Temperatures for Actuation Applications. *Sensors* **2023**, *23*, doi:10.3390/s23010299.
26. Czyż, O.; Kusiński, J.; Radziszewska, A.; Liao, Z.; Zschech, E.; Kąc, M.; Ostrowski, R. Study of Structure and Properties of Fe-Based Amorphous Ribbons after Pulsed Laser Interference Heating. *J Mater Eng Perform* **2020**, *29*, 6277–6285, doi:10.1007/s11665-020-05109-w.

27. Zhang, J.; Shan, G.; Li, J.; Wang, Y.; Shek, C.H. Structures and Physical Properties of Two Magnetic Fe-Based Metallic Glasses. *J Alloys Compd* **2018**, *747*, 636–639, doi:10.1016/j.jallcom.2018.03.085.
28. Li, Y.; Chen, W. zhi; Dong, B. shao; Zhou, S. xiong Effects of Phosphorus and Carbon Content on the Surface Tension of FeSiBPC Glass-Forming Alloy Melts. *J Non Cryst Solids* **2018**, *496*, 13–17, doi:10.1016/j.jnoncrysol.2018.05.016.
29. Li, T.X.; Li, R.; Lin, Y.; Bu, F.; Li, J.; Li, K.; Hu, Z.; Ju, L. Study of Enhanced Magnetoelectric Coupling Behavior in Asymmetrical Bilayered Multiferroic Heterostructure with Two Resonance Modes. *J Alloys Compd* **2022**, *895*, 162674, doi:https://doi.org/10.1016/j.jallcom.2021.162674.
30. Kabacoff, L.T. Thermal, Magnetic, and Magnetomechanical Properties of Metglas 2605 S2 and S3. *J Appl Phys* **1982**, *53*, 8098–8100, doi:10.1063/1.330270.
31. Lopatina, E.; Soldatov, I.; Budinsky, V.; Marsilius, M.; Schultz, L.; Herzer, G.; Schäfer, R. Surface Crystallization and Magnetic Properties of Fe84.3Cu0.7Si4B8P3 Soft Magnetic Ribbons. *Acta Mater* **2015**, *96*, 10–17, doi:10.1016/j.actamat.2015.05.051.
32. Ok, H.N.; Morrish, A.H. Origin of the Perpendicular Anisotropy in Amorphous Fe82B12Si6 Ribbons. *Phys Rev B* **1981**, *23*, 2257–2261, doi:10.1103/PhysRevB.23.2257.
33. Gemperle, R.; Kraus, L.; Kroupa, F.; Schneider, J. Influence of Surface Oxidization on Induced Anisotropy of Amorphous (FeNi) PB Wires. *physica status solidi (a)* **1980**, *60*, 265–272, doi:https://doi.org/10.1002/pssa.2210600131.
34. Ok, H.N.; Morrish, A.H. Amorphous-to-Crystalline Transformation of Fe82B12Si6. *Phys Rev B* **1980**, *22*, 3471–3480, doi:10.1103/PhysRevB.22.3471.
35. Keupers, A.; De Schepper, L.; Knuyt, G.; Stals, L.M. Chemical and Topological Short Range Order in Amorphous Fe40Ni38Mo4B18 (Metglas 2826MB). *J Non Cryst Solids* **1985**, *72*, 267–278, doi:https://doi.org/10.1016/0022-3093(85)90183-8.
36. Morito, N. Surface Crystallization Induced by Selective Oxidation of Boron in Fe-B-Si Amorphous Alloy. *Key Eng Mater* **1990**, *40–41*, 63–68, doi:10.4028/www.scientific.net/KEM.40-41.63.
37. Herzer, G. Magnetomechanical Damping in Amorphous Ribbons with Uniaxial Anisotropy. *Materials Science and Engineering: A* **1997**, *226–228*, 631–635, doi:https://doi.org/10.1016/S0921-5093(96)10697-3.
38. Tong, X.; Zhang, Y.; Wang, Y.; Liang, X.; Zhang, K.; Zhang, F.; Cai, Y.; Ke, H.; Wang, G.; Shen, J.; et al. Structural Origin of Magnetic Softening in a Fe-Based Amorphous Alloy upon Annealing. *J Mater Sci Technol* **2022**, *96*, 233–240, doi:https://doi.org/10.1016/j.jmst.2021.01.098.
39. Stoyanov, P.G.; Grimes, C.A. A Remote Query Magnetostrictive Viscosity Sensor. *Sens Actuators A Phys* **2000**, *80*, 8–14, doi:https://doi.org/10.1016/S0924-4247(99)00288-5.
40. Herrero-Gómez, C.; Marín, P.; Hernando, A. Bias Free Magnetomechanical Coupling on Magnetic Microwires for Sensing Applications. *Appl Phys Lett* **2013**, *103*, 142414, doi:10.1063/1.4821777.
41. Hernando, A.; Madurga, V.; Barandiarán, J.M.; Liniers, M. Anomalous Eddy Currents in Magnetostrictive Amorphous Ferromagnets: A Large Contribution from Magnetoelastic Effects. *J Magn Magn Mater* **1982**, *28*, 109–116, doi:https://doi.org/10.1016/0304-8853(82)90034-8.
42. Gutiérrez, J.; Barandiarán, J.M.; Nielsen, O. V Magnetoelastic Properties of Some Fe-Rich Fe Co Si B Metallic Glasses. *physica status solidi (a)* **1989**, *111*, 279–283, doi:https://doi.org/10.1002/pssa.2211110129.
43. Leung, C.M.; Zhuang, X.; Xu, J.; Li, J.; Zhang, J.; Srinivasan, G.; Viehland, D. Enhanced Tunability of Magneto-Impedance and Magneto-Capacitance in Annealed Metglas/PZT Magnetoelectric Composites. *AIP Adv* **2017**, *8*, 055803, doi:10.1063/1.5006203.
44. Kaczkowski, Z.; Vlasák, G.; Švec, P.; Duhaj, P.; Ruuskanen, P.; Barandiarán, J.M.; Gutiérrez, J.; Minguez, P. Influence of Heat-Treatment on Magnetic, Magnetostrictive and Piezomagnetic Properties and Structure of Fe64Ni10Nb3Cu1Si13B9 Metallic Glass. *Materials Science and Engineering: A* **2004**, *375–377*, 1065–1068, doi:https://doi.org/10.1016/j.msea.2003.10.082.
45. Setiadi, R.N.; Schilling, M. Sideband Sensitivity of Fluxgate Sensors Theory and Experiment. *Sens Actuators A Phys* **2019**, *285*, 573–580, doi:https://doi.org/10.1016/j.sna.2018.11.049.
46. Savage, H.; Clark, A.; Powers, J. Magnetomechanical Coupling and ΔE Effect in Highly Magnetostrictive Rare Earth - Fe2compounds. *IEEE Trans Magn* **1975**, *11*, 1355–1357, doi:10.1109/TMAG.1975.1058791.
47. Egami, T. Structural Relaxation in Amorphous Fe40Ni40P14 B6 Studied by Energy Dispersive X-Ray Diffraction. *J Mater Sci* **1978**, *13*, 2587–2599, doi:10.1007/BF02402745.
48. Herzer, G. Effect of Domain Size on the Magneto-Elastic Damping in Amorphous Ferromagnetic Metals. *International Journal of Materials Research* **2022**, *93*, 978–982.

49. Egami, T. Structural Relaxation in Amorphous Alloys - Compositional Short Range Ordering. *Mater Res Bull* **1978**, *13*, 557–562, doi:https://doi.org/10.1016/0025-5408(78)90178-2.